ANALYSIS OF A CONTACTLESS AIR FILM CONVEYOR USING A VISCOUS TRACTION PRINCIPLE

Wei ZHONG*, Jia WANG and Fanghua LIU

*School of Mechanical Engineering, Jiangsu University of Science and Technology
Mengxi Road 2, Zhenjiang, Jiangsu, 212003 China
(E-mail: zhongwei@just.edu.cn)

Abstract. Many industries require contactless transport of delicate or clean products. In this study, a contactless air film conveyor for flat objects is introduced. The object is supported by a thin film formed between the object and the conveyor surface and transported by viscous traction which is generated by controlled airflow underneath the object. Experiments are conducted to investigate the viscous force, which decreases as the increase of gap thickness. A simplified model is established to help characterize the viscous force. The calculated results show a good agreement with the experimental data. It is revealed that the viscous force is the resultant of an actuating force in the pocket and side areas and a drag force from airflow across the dam area. Simulation and experiments are conducted using a hybrid controller for one dimension position control. The results verify the effectiveness of the theoretical modeling and the control method.

Keywords: Air film conveyor, viscous force, position control, air film

INTRODUCTION

Many industries require contactless transport of delicate or clean products such as silicon wafers, flat foodstuffs and freshly painted objects. The pneumatic levitation has become dominate in the non-contact conveying field, and, two different pneumatic methods can be considered: vacuum chucks [1, 2], or, air cushion [3]. The non-contact vacuum chucks provide an upward lifting force and thereby can pick-and-place a workpiece. The air-cushion method commonly uses arrays of orifices or porous pads to supply pressurized air beneath the workpiece to form an air film for support [4, 5].The forward movement is actuated by an external force using an additional positioning stage. However, these two methods can hardly completely avoid mechanical contact and thus bring risk of breakage or contamination to the products in actual applications [6]. Moreover, existence of the moving guides might also destroy the cleanliness of the environment.

Airflow across the surface of an object induces shear stress at the boundary and this might be used as an actuating force. Delhaes [7] introduced a combined motor-bearing unit whose spindle is driven by both viscous force and bearing force. In these cases, airflow produces a viscous force in addition to the air cushion to generate an actuating torque. Likewise, the same principle can be applied to linear motion. Many researchers used tilted air jets relative to the surface to get the aim. Paivanas et al. [8] described a system for wafer handling and transport applications using inclined air jets. Biegelsen et al. [9] developed a paper mover using 1152 directed air jets in a 12 in×12 in array. Fukuta et al. [10] presented an array of MEMS-based actuators for distributed micromanipulation by generating and controlling the air-flow force field. However, it should also be noted that air jets easily induce disturbance and electrostatic contamination problems.

Other than tilted air jets, some researchers used aerodynamic-traction principle to move objects. Moon and Luntz [11] accomplished this by generating the manipulation flow field on the top surface of an object while a standard air table generates air cushion for support. Delettre [12] developed a 120 mm × 120 mm positioning system which uses individually controlled vertical jets for propulsion. Laurent et al. [13] utilized this system to perform experiments with different objects, and found that the system works better for heavy objects over light objects. Objects of different weights float at different heights so that it is important to discuss the relationship between viscous force and gap thickness. However, Laurent et al. did not report such results. Ku et al. [14] developed a surface device using a 4 mm × 4 mm array of 100 capillary glass tubes to generate a pressure field. Each tube was individually connected to a two-position valve to provide positive or negative pressures. Rij and Wesselingh [15, 16] developed the same idea but they set specific actuator cells in order to produce horizontal airflow underneath the workpiece. The prototype of the device they developed is very small in size and only applied to micro-positioning. In this study, we used a similar design and established a simple model. The control method and positioning results are presented.

DESCRIPTION OF THE AIR FILM CONVEYOR

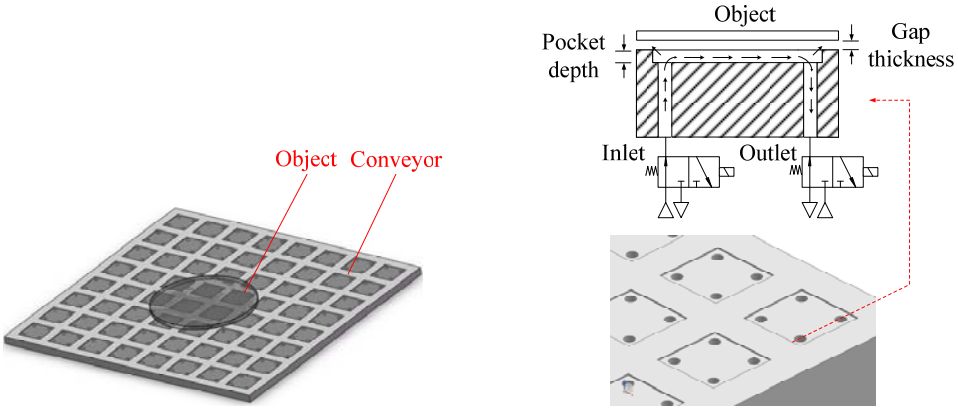

(a) General view (b) Cutaway view showing the working principle

FIGURE 1. Air film conveyor.

Figure 1(a) schematically shows a general view of the air film conveyor. A flat object is supported by a thin film formed between the object and the conveyor surface, and, it can be transported on the conveyor using controlled airflow underneath the object. Figure 1(b) illustrates the working principle. Each port is connected to an independent solenoid valve (3/2 normally closed valve) to select positive pressure or negative pressure as required. Pressure at the inlet ports is certainly larger than that at the outlet ports. Due to the pressure difference a horizontal airflow is generated in the pocket and thus produces a viscous force. Therefore, the floating object can be transported without friction along the airflow direction.

MATHEMATICAL MODELING

A three-dimensional Cartesian coordinate is built in the representative region. The length and width directions are denoted as x-y coordinate, and the film thickness direction is denoted as z coordinate. The actuating force is considered only in the direction of airflow in the pockets, i.e., the x-direction. Consequently, the film flow behavior is described using Navier-Stokes equations, which in x-direction is simplified as below

$$-\frac{\partial p}{\partial x}+\mu\frac{\partial^2 u}{\partial z^2}=0 \tag{1}$$

where p is the film pressure, μ is the air viscosity, and u is the flow velocity in the gap.

Integrating equation (1) with respect to z, with the boundary condition that u=0 (z=0) and u=V_0 (z=h), we obtain the expression of velocity in the pocket area as below

$$u=\frac{p_2-p_1}{2\mu l}\left(z^2-hz\right)+\frac{V_0}{h}z \tag{2}$$

where p_1 is the film pressure at the inlet, p_2 is the film pressure at the outlet, and l is the length of the pocket.

For Newtonian fluids, the shear stress τ is linearly proportional to the velocity gradient as below

$$\tau=-\mu\frac{\partial u}{\partial z} \tag{3}$$

Figure 2 (a) shows a typical actuating cell which is divided into three areas. They are pocket area, dam area and side area. It is assumed that the airflow in the pocket and side areas is in the x-direction, while that across the dam area is opposite. The total force is considered as the resultant of an actuating force resulted from the airflow in the pocket and side areas and a drag force resulted from airflow across the dam area.

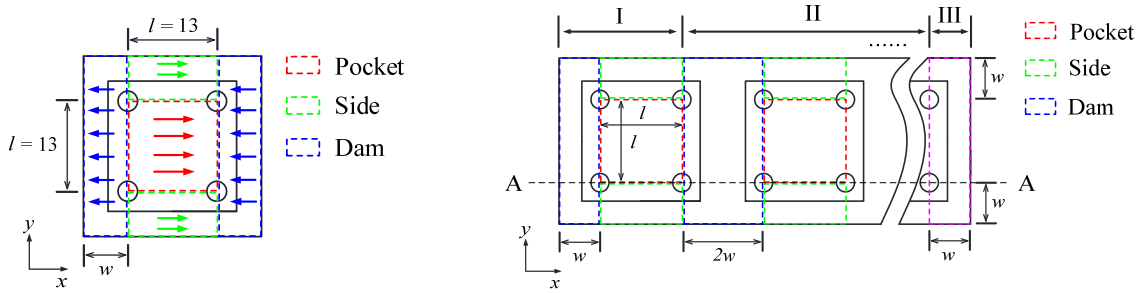

(a) Region segmentation of a typical actuating cell (b) Region segmentation of a representative row

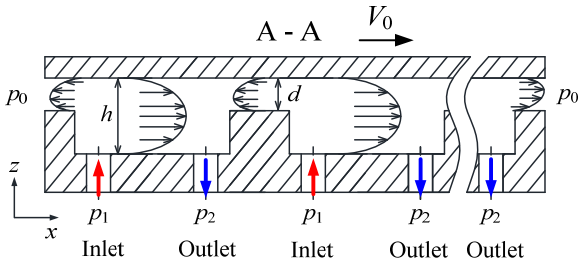

(c) Velocity profile in the gap

FIGURE 2. Modeling of airflow in the gap formed by the object and the conveyor surface.

Submitting equation (2) into equation (3) with the boundary condition that $z=h$ obtains the shear stress τ_p applied by air on the surface in the pocket area.

$$\tau_p = \frac{p_1 - p_2}{l}\frac{h}{2} - \frac{\mu}{h}V_0 \tag{4}$$

For the dam area and side area, the film height is denoted as d. Similarly, the shear stress τ_d in the dam area is obtained as

$$\tau_d = -\left(\frac{p_1 - p_2}{2w}\frac{d}{2} + \frac{\mu}{d}V_0\right) \tag{5}$$

And, the shear stress τ_s in the side area is thus represented as

$$\tau_s = \frac{p_1 - p_2}{l}\frac{d}{2} - \frac{\mu}{d}V_0 \tag{6}$$

Further analysis is conducted within a representative row as shown in Figure 2(b). Three zones, designated as I, II and III, are separated to respectively calculate the viscous force. Zone I is the leftmost unit containing a pocket area, a dam area and two side areas. Zone II contains three middle reduplicate units similar to that of zone I and zone III is only the rightmost dam area. For zone I, the viscous force F_p, F_d and F_s in the pocket, dam and side areas can be respectively calculated by Eqs. (7) (8) (9), and the total force F_1 is calculated by $F_p + F_d + F_s$.

$$F_p = \frac{p_1 - p_2}{2}hl - \frac{\mu}{h}V_0 l^2 \tag{7}$$

$$F_d = -\left(\frac{p_1 - p_0}{w}\frac{d}{2} + \frac{\mu}{d}V_0\right)\cdot\left[w\cdot(l+2w)\right] \tag{8}$$

$$F_s = \left(\frac{p_1 - p_2}{l}\frac{d}{2} - \frac{\mu}{d}V_0\right)\cdot 2wl \tag{9}$$

For a single unit in zone II, the viscous force in the pocket, dam and side regions can be respectively calculated by Eqs. (10) (11) (12), and the total force F_2 is calculated by $F_p + F_d + F_s$.

$$F_p = \frac{p_1 - p_2}{2}hl - \frac{\mu}{h}V_0 l^2 \tag{10}$$

$$F_d = -\left(\frac{p_1 - p_2}{2w}\frac{d}{2} + \frac{\mu}{d}V_0\right)\cdot\left[2w\cdot(l+2w)\right] \tag{11}$$

$$F_s = \left(\frac{p_1 - p_2}{l}\frac{d}{2} - \frac{\mu}{d}V_0\right)\cdot 2wl \tag{12}$$

For zone III, the viscous force in the dam area can be calculated as below

$$F_3 = F_d = -\left(\frac{p_0 - p_2}{w}\frac{d}{2} + \frac{\mu}{d}V_0\right)\cdot\left[w\cdot(l+2w)\right] \tag{13}$$

Equations given above suggest that the pressure difference p_1-p_2 is necessary for the calculation of viscous force. Integrating equation (2) with respect to cross-sectional area, the volumetric flow rate Q_p in the pocket area is thus expressed as

$$Q_p = \frac{p_1 - p_2}{12\mu}h^3 + \frac{hl}{2}V_0 \tag{14}$$

Equation (14) indicates that the pressure difference p_1-p_2 can be obtained according to the amount of horizontal airflow in the pocket. However, objectively, this flow rate is almost impossible to be accurately measured. Furthermore, variation of the gap thickness might also exert influence on it. Considering the

influences from inlet flow, outlet flow and gap thickness, a fitting equation is proposed to approximate the flow rate Q_p as follows

$$Q_p = \alpha\left(Q_1 + Q_2\right)\left(\frac{d_0}{d_0 + \delta d}\right)^n \tag{15}$$

where Q_1 is the inlet flow rate, Q_2 is the outlet flow rate, α and n are correction factors, d_0 is the initial film thickness and δd is the changed thickness.

Therefore, the total viscous force is considered as the sum of zone I, II and III. That is, for the case of the representative region including 25 actuating cells (5×5), the total viscous force F can be calculated as below

$$F = 5F_1 + 20F_2 + 5F_3 \tag{16}$$

EXPERIMENTAL METHODS

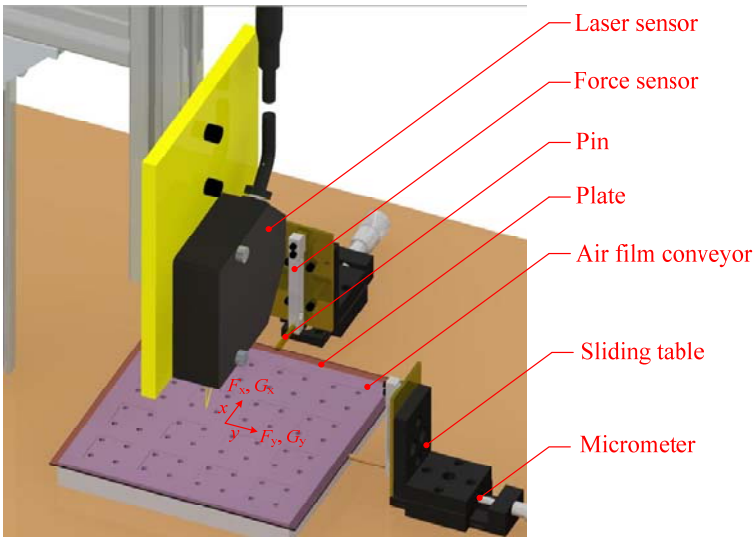

FIGURE 3. Apparatus for viscous force measurement.

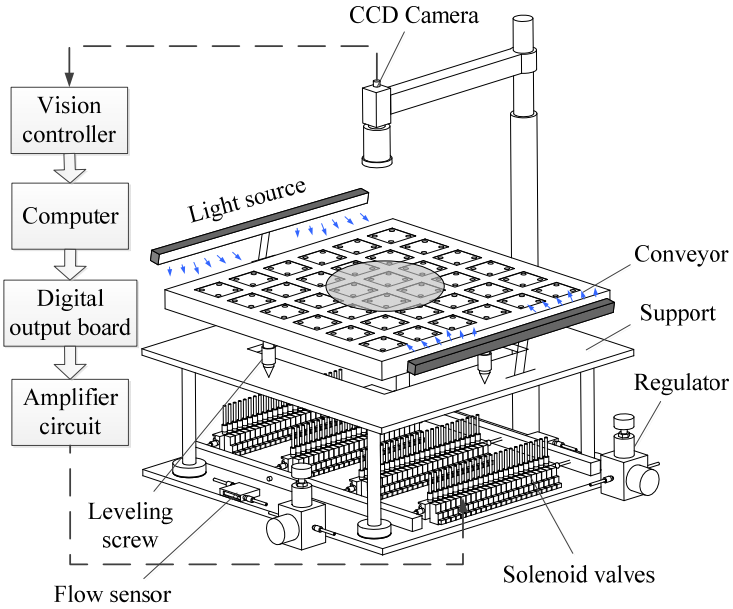

FIGURE 4. Experimental setup for position control.

Figure 3 schematically shows the apparatus used for measuring the viscous force. A square plate sized 80 × 80 mm is supported by the air film upon the conveyor surface. Two pins are connected to two force sensors (CZT600-20G, SHANDONG SCALE Co., Ltd), respectively. The force sensors are respectively placed on two sliders, and the position of the plate can be finely adjusted by turning the micrometers. The test air film conveyor unit is mounted on a slight tilt so that the two pins tightly touch the side of the plate. Thus, the viscous

force F_x and F_y can be obtained by subtracting the components of gravity G_x and G_y from the reading of the force sensors, respectively. Moreover, the gap thickness can be directly detected by the laser sensor (LK-G30, Keyence Co., Ltd). In this way, to open or close appropriate valves, the viscous force can be measured in two perpendicular directions, and the results are averaged in order to reduce uncertainty.

Figure 4 shows the experimental setup for contactless position control of an object upon the conveyor surface. Compressed air is supplied and regulated to appropriate pressure. A vacuum circuit is created using a vacuum pump and a vacuum regulator is in use. Each port is individually connected to the air circuit and the vacuum circuit by switching the solenoid valves (ESO-3B-12-L2, Clippard Co.,Ltd). Two thermal-type flow sensors (FPM711, SMC Co., Ltd) are installed to show the flow rate in the air circuit and the vacuum circuit, respectively. A CCD Camera is placed above the conveyor to take image of the surface in order to obtain the position of the object, and light sources are installed to improve the effect of vision detection. A vision controller (CV-X150A, Keyence Co., Ltd) is used to process the images at the rate of 20 frames per second. A software package is developed on the computer using VC++ to receive data from the vision controller, display real-time results and control the valves. Electrical control signals are sent by computer via multi-channel digital output boards (PCI-1758UDO, Advantech Co., Ltd).

1D-position control is focused in this work. Particularly, all the inlet or outlet ports of a same column are classified into a group and controlled simultaneously. So, different combinations of columns with positive or negative pressure can be realized. However, not all combinations work well. Only when the inlet ports of a same column are supplied with positive pressure while outlet ports negative pressure can the object be moved effectively, and in this case, such column of cells is named active actuating column. Meanwhile, the active actuating column should be covered by the object, otherwise it is ineffective. Naturally, the actuating force can be enlarged as the number of active actuating columns increases. Experiments are performed to verify this. Figure 5 shows the measured position versus time in the case that the active actuating column is numbered 3, 4 and 5, respectively. The object is a circular plate with a diameter of 90 mm and a weight of 103.5 g. Evidently, the object exhibits a larger velocity as the column number increases, and the velocity at 4 s is estimated around 17 mm/s, 31 mm/s and 52 mm/s for the three cases. Moreover, the object can of course slow down or reverse motion by switching the positive and negative pressure for appropriate ports.

As a result, the control signal can be defined as the number of active actuating columns underneath the object. Figure 6 shows examples of the control signal from +5 to -5. A small filled black circle represents a port connected to negative pressure and the empty circle connected to positive pressure. Note that the control signal is an integer. Furthermore, it is saturated, and the saturation depends on the relation of the surface geometry and the object size. The range of ±5 is limited because the selected object just covers 5 columns of the actuating cells.

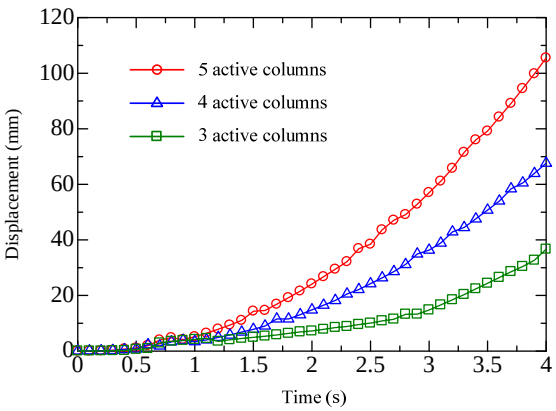

FIGURE 5. Position versus time with different active columns.

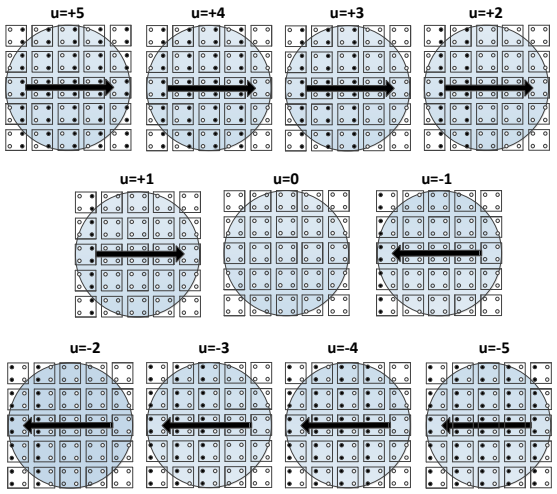

FIGURE 6. Representation of control signal.

SIMULATION AND EXPERIMENTAL RESULTS

A hybrid controller, which consists of bang-bang control and fuzzy PID control, is constructed to obtain precise control performance. The bang-bang controller is used when the object is far from the desired position. Otherwise, fuzzy PID controller is used when the object is close to the desired position. Position of the object on the conveyor surface is obtained by the vision sensor, and the error between the measured signal and the reference signal is used as the feedback. The overall structure of the hybrid controller is shown in Fig. 7. The initial values of the coefficients Kp, Ki and Kd are obtained by trial-and-error in order to find a good trade-off

between rise time, overshoot and stability. The control signal calculated by the controller is rounded to an integer, which denotes the number of the active actuating columns.

The input variables for the fuzzy PID controller are defined as: $e=y_{ref}-y$ and de/dt. Real interval of the variables is obtained by using scaling factors which are E and Ec. The fuzzy control rule is in the form of: IF e=Ei and de=dEj THEN Uv=Uv(i,j). These rules are written in a rule base look-up table, which is shown in Table 1. The rule base structure is Mamdani type. All of the variables are implied as linguistic values and defined with the 7 linguistic values. The values are: NB-negative big, NM-negative medium, NS-negative small, Z-zero, PS-positive small, PM-positive medium, PB-positive big. Each linguistic value is represented as triangular membership function (Fig. 8). Thus, e and de variables are converted to fuzzy logic linguistic variables. Variables are defined in interval of [-3, 3]. Rule base was determined by using experience and engineering mentality.

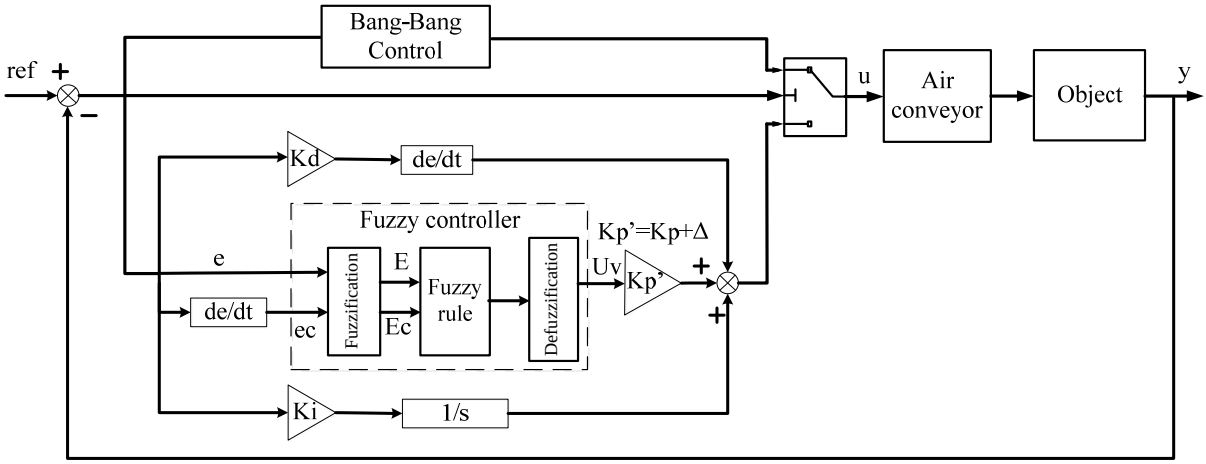

FIGURE 7. Control structure.

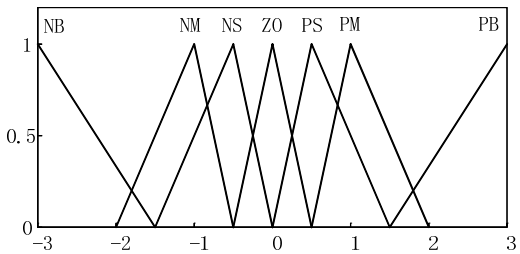

FIGURE 8. Membership function.

TABLE 1. Rule base for fuzzy logic control

de/e	NB	NM	NS	ZO	PS	PM	PB
NB	PB	PB	PM	PM	PS	ZO	ZO
NM	PB	PB	PM	PS	PS	ZO	NS
NS	PM	PM	PM	PS	ZE	NS	NS
ZO	PM	PM	PS	ZO	NS	NM	NM
PS	PS	PS	ZO	NS	NS	NM	NM
PM	PS	ZO	NS	NM	NM	NM	NB
PB	ZO	ZO	NM	NM	NM	NB	NB

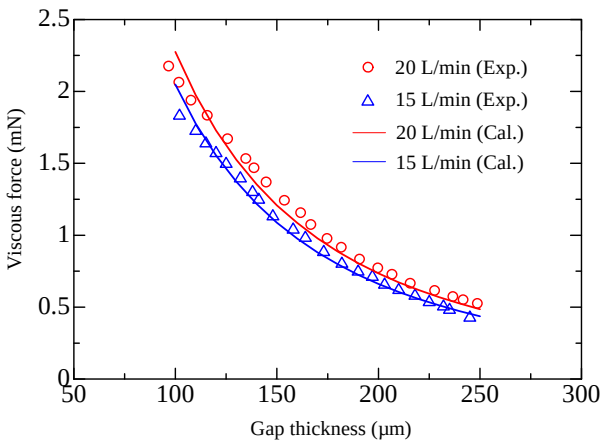

FIGURE 9. Viscous force versus gap thickness.

Figure 9 plots the measured viscous force against gap thickness when Q_2 is set to 15 L/min and 20 L/min while Q_1 is 30 L/min. The floating height of the plate can be adjusted by slowly changing the load mass (cf.

Figure 3). Clearly, the viscous force increases as the gap thickness decreases. Especially for narrow gaps, the viscous force is strongly influenced by thickness variation. Reduction of the gap thickness accelerates the airflow in the pockets so that it produces a larger viscous force. On the other hand, the viscous force increases with the suction flow rate under a given gap thickness. Calculated results are provided for a comparison, and the coefficients of α and n are identified with a value of 0.25 and 0.8, respectively. It is found that the calculated curves can correctly predict the trend of the experimental data, and the relative error evaluated by the root-sum-square method is 6.2% and 4.1% for the cases of Q_2 = 20 L/min and Q_2 = 15 L/min, respectively.

TABLE 2. Experimental step response performance of the controller with different objects

Object	Mass (g)	Step amplitude (mm)	Kp	Ki	Kd	Rise time (s)	Overshoot	Static error (mm)
A	87.6	35	0.72	0.04	0.51	1.6	0.11%	0.20
B	103.5	35	0.72	0.04	0.51	1.5	1.74%	0.15

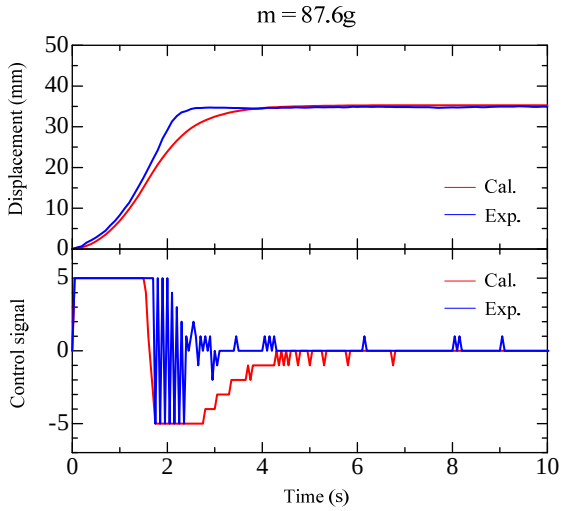

FIGURE 10. Step response and control signal (m = 87.6 g).

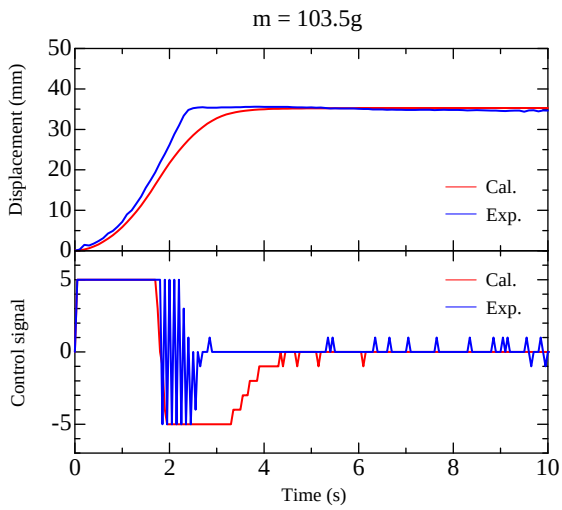

FIGURE 11. Step response and control signal (m = 103.5 g).

To verify the effectiveness of the theoretical modeling and control method, two objects, designated as A and B, are used for position control experiment. The objects are circular plates with a same diameter of 90 mm and a weight of 87.6 and 103.5 g. The supply flow rate is initially set to 85 L/min while the vacuum flow rate is 10.5 L/min throughout the experiment. An extremely smooth wall is set to keep the levitated object always moving along a straight line, and the friction between the two is negligibly small because of a line contact. Figure 10 and Figure 11 show the calculated and experimental results of a step response and the control signal, and the performances are summarized in Table 2. No apparent overshoot is observed for any of the objects and the maximum static error is about 0.2 mm. However, if a classical PID controller was used, it might give good performance for one object but is not robust to variations of the physical properties such as weight and geometry. That is to say, it is difficult to guarantee all the performances simply using the same PID parameters for those objects with different weight. It should also be noted the used fuzzy PID controller offers advantages for objects with only a small difference in weight. Moreover, the comparison shows that the real viscous force is larger than that of the calculation. Anyway, the results verify the feasibility of the mathematical model and the control method.

CONCLUSIONS

In this study, a contactless air film conveyor for supporting and moving flat objects is introduced. The viscous force is experimentally studied. It is found that the viscous force decreases as the gap thickness is increased and increases if the suction flow rate is enlarged. The viscous force induced on the surface is considered as the resultant of an actuating force resulted from the air flow in the pocket and side areas and a drag force from air flow across the dam area. A simplified model that characterizes the film flow behavior is proposed, and it is confirmed that the model can accurately predict the experimental results of viscous force versus gap thickness. A hybrid controller consisting of bang-bang control and fuzzy PID control is used for 1D-position control, with the number of active actuating column as the control signal. The results for different flat objects verify the performance of the conveyor system.

ACKNOWLEDGMENTS

This study was supported by the National Natural Science Foundation of China (Grant No. 51675247).

REFERENCES

1. LI, X., et al., Development of a pneumatic sucker for gripping workpieces with rough surface, IEEE Transactions on Automation Science and Engineering, Vol. 13(2), 2016, pp. 639-646.
2. BRUN, X.F., MELKOTE, S.N., Modeling and Prediction of the Flow, Pressure, and Holding Force Generated by a Bernoulli Handling Device, ASME Journal of Manufacturing Science and Engineering, Vol. 131, pp. 031018-1-7, 2009.
3. ZHONG, W., et al., Study on the basic characteristics of a contactless air film conveyor using viscous traction, Proc IMechE Part J: J Engineering Tribology, Vol. 230(9), 2016, pp. 1139-1148.
4. LEE, H.G., LEE, D.G., Design of a large LCD panel handling air conveyor with minimum air consumption, Mechanism and Machine Theory, Vol. 41, pp. 790-806, 2006.
5. AMANO, K., YOSHIMOTO, S., MIYATAKE, M., HIRAYAMA, T., Basic investigation of noncontact transportation system for large TFT-LCD glass sheet used in CCD inspection section, Precis. Eng., Vol. 35, pp. 58-64, 2011.
6. BRUN, X.F., MELKOTE, S.N., Analysis of stresses and breakage of crystalline silicon wafers during handling and transport, Solar Energy Materials and Solar Cells, Vol. 93(8), pp. 1238–1247, 2009.
7. DELHAES, G.M.J., VAN BEEK, A., VAN OSTAYEN, R.A.J., SCHMIDT, R.H.M., The viscous driven aerostatic supported high-speed spindle, Tribology International, Vol. 42, pp. 1550–1557, 2009.
8. PAIVANAS, J.A., HASSAN, J.K., Air film system for handling semiconductor wafers, IBM Journal of Research and Development, Vol. 23, pp. 361–375, 1979.
9. BIEGELSEN, D., BERLIN, A., CHEUNG, P., FROMHERZ, M., GOLDBERG, D., JACKSON, W., PREAS, B., REICH, J., SWARTZ, L., Airjet paper mover, Proc. SPIE Int. Symposium on Micromachining and Microfabrication, USA, 4176, pp. 122-129, 2000
10. FUKUTA, Y., CHAPUIS, Y.A., MITA, Y., FUJITA, H., Design, Fabrication, and Control of MEMS-Based Actuator Arrays for Air-Flow Distributed Micromanipulation, Journal of Microelectromechanical Systems, Vol. 15, pp. 912-926, 2006
11. MOON, H. LUNTZ, J., Distributed manipulation of flat objects with two airflow sinks, IEEE Transactions on Robotics, Vol. 6, pp. 1189–1201, 2006.
12. DELETTRE, A., LAURENT G.J., LE FORT-PIAT, N., A new contactless conveyor system for handling clean and delicate products using induced air flows, IEEE/RSJ International Conference on Intelligent Robots and Systems (IROS), Taiwan, pp. 2351–2356, 2010
13. LAURENT, G.J., DELETRRE, A., LE FORT-PIAT, N., A new aerodynamic traction principle for handling products on an air cushion, IEEE Transactions on Robotics, Vol. 27, pp. 379-384, 2011.
14. KU, P.J., WINTHER, K.H., STEPHANOU, H.E., Distributed control system for an active surface device, Proceedings 2001 ICRA, IEEE International Conference on Robotics and Automation, vol. 4, pp. 3417–3422, 2001.
15. VAN RIJ, J., WESSELINGH, J., VAN OSTAYEN, R.A.J., SPRONCK, J.W., SCHMIDT, R.H.M., VAN EIJK, J., Planar flat product transport using viscous traction, Proceedings of the STLE/ASME International Joint Tribology Conference. USA, October 2008.
16. VAN RIJ, J., WESSELINGH, J., VAN OSTAYEN, R.A.J., SPRONCK, J.W., SCHMIDT, R.H.M., VAN EIJK, J., Planar wafer transport and positioning on an air film using a viscous traction principle, Tribology International, Vol. 42, pp. 1542–1549, 2009.

